



TECHNICAL ARTICLE

Investigation into Hypo-eutectic, Eutectic, and Hyper-eutectic Compositions of Al-xCu Alloys Produced by the Powder Metallurgy Method

Mustafa Doğan and Uğur Avcı

Submitted: 5 June 2022 / Revised: 4 November 2022 / Accepted: 17 December 2022 / Published online: 3 January 2023

In this study, characteristic changes of Al-xCu alloys produced by the powder metallurgy method in critical transformation regions of binary Al-Cu phase diagram were investigated. In this framework, Al-xCu alloys with a content of 5-15-25-33-45 wt.% Cu, which would enable the formation of hypo-eutectic, eutectic, and hyper-eutectic regions, were prepared. The prepared powders were converted into a green compact form by compressing at a 600 MPa pressure ratio. The obtained green samples were placed in the sintering die and sintered in accordance with the critical transformation temperatures determined in the binary phase diagram. Once the sintering process was completed, the samples in the hot die were compressed at a pressure ratio of 5 MPa and cooled with air. As a result of the microstructural examinations on the produced samples, it was observed that partial liquefaction occurred in the Cu particles due to the increase in the Cu content of the alloy and the amount of CuAl₂ intermetallic compound increased accordingly. In this context, as the Cu content of Al-xCu alloys increased, the microhardness and wear resistance values increased; however, the ductility, compressive strength and electrical conductivity values decreased.

Keywords Al-xCu alloys, microstructure, powder metallurgy, sintering process

1. Introduction

Aluminum alloys are widely used in many areas of the industry due to their strength-to-weight ratio, high electrical and thermal conductivity, as well as good corrosion resistance (Ref 1-3). However, pure Al material does not have sufficient mechanical properties, so it is used by alloying with many elements or combining with other materials (Ref 4-6). Copper is one of the elements with relatively high solubility in aluminum. Therefore, it offers the opportunity to obtain an alloy with new characteristic properties by adding it to Al in varying proportions (Ref 7, 8). In studies on Al-Cu alloys, it has been determined that CuAl₂ secondary phases are formed and these phases affect the microstructure, mechanical and physical properties of the material (Ref 9-11). In addition, it was observed that more CuAl₂ intermetallic compounds were formed in proportion to the increase in Cu content in Al-Cu alloys (Ref 12).

Since Al-Cu mixture powders can be shaped with low pressure, do not require high temperatures during the sintering process, and are easily accessible, it has become quite common to convert them into final products by powder metallurgy (PM)

method, which is an environmentally friendly production model. The most important factor affecting the characteristics of the samples produced by the PM method is the density values after sintering. In this context, in the study conducted on elementary alloy samples (AA2024) produced from Al and Cu powders, the relative density values obtained after sintering at 460 and 560 °C for an hour were 94.97 and 97.12%, respectively (Ref 13). In addition, in the study conducted on the alloy produced by adding 2-4-6 wt.% Cu to Al, the relative density value decreased with the increase in the Cu content but increased with the increase in the compaction pressure ratio (Ref 14).

The $\alpha \rightarrow$ (Al-rich phase) region in the binary Al-Cu phase diagram dissolves a maximum of 5.65wt.%Cu at the eutectic temperature (548 °C). As a result of this situation, values close to the maximum dissolution ratio in the α region were used to determine the Cu content in most studies on Al-Cu alloys (Ref 15, 16). In studies using the casting method, changes in hypo-eutectic, eutectic and hyper-eutectic regions were rarely investigated by increasing the Cu content (Ref 17, 18).

In the light of the abovementioned information, it has been concluded that investigating the microstructure, mechanical and physical properties of Al-Cu alloys produced at different rates using the PM method will be effective regarding the development of alloy materials. In this context, this study aims to examine the interaction of the alloy ratios in the critical transformation regions of the binary Al-Cu phase diagram at the determined sintering temperatures and the changes in the characteristic properties of the material as a result of this interaction. It has been observed that there are many studies on critical transformation regions to examine the conditions in the solidification process of Al-Cu alloys produced by the casting method. However, studies on the use of these regions in the sintering process are limited. The present study can contribute

Mustafa Doğan and Uğur Avcı, Material Science and Engineering, Kahramanmaraş Sutcu Imam University, 46100 Kahramanmaraş, Turkey. Contact e-mails: mustafa4064@hotmail.com and ogrtmugav@gmail.com.

to the production of Al-Cu alloys by the PM method and the understanding of sintering processes.

2. Experimental Procedure

2.1 Determination of Alloy Ratios and Sintering Temperatures

One of the parameters that forms the basis of PM studies and plays a decisive role in the general properties of the produced samples is the alloy ratio. In this study, binary Al-Cu phase diagram was used to determine the alloy ratio and it was planned to produce samples in critical regions on the diagram. In the phase diagram shown in Fig. 1, it is seen that different phase formations occur with the increase in Cu content and temperature change. The eutectic transformation point is located on the horizontal line at 548 °C, called the critical transformation line, and this point intersects with a 33% copper content. At this transformation point, it is seen that the liquid phase transforms into two different solid phases ($\alpha + \theta$) during cooling. On the left side of this transformation point, there is the hypo-eutectic region ($\alpha + L$), and on the right side, the hyper-eutectic region ($\theta + L$). In this research, since it was planned to produce Al-Cu alloys in the hypo-eutectic, eutectic and hyper-eutectic regions by PM method, Al powder was mixed with Cu powders at a rate of 5-15-25-33-45 wt.%.

To determine the sintering temperatures of Al-xCu alloys, the lower (T_{low}) and upper (T_{up}) transformation limit temperatures in the regions determined in the binary phase diagram were considered. However, high sintering temperatures to be applied to alloys are likely to cause dimensional changes in the samples (Ref 19). It was concluded that partial liquefaction in alloys would be appropriate to limit this dimensional change. Thus, depending on the Cu content, the transformation limit

temperatures in the region were determined and the sintering temperature (T_s) was calculated according to Eq 1.

$$T_s = T_{low} + \frac{T_{up} - T_{low}}{4} \quad (\text{Eq 1})$$

In this context, the sintering temperatures of Al-5-15-25Cu alloys in the hypo-eutectic region were determined as 575, 565 and 555 °C, respectively. In addition, the sintering temperature of the Al-33Cu alloy in the eutectic point was determined as 548 °C, and the sintering temperature of the Al-45Cu alloy in the hyper-eutectic region was determined as 555 °C.

In the preliminary study on the determination of the sintering temperature and time of the pure Al sample, it was determined that the ideal sintering temperature was 600 °C and the ideal sintering time was 45 min (Ref 20). Depending on this situation, the sintering time of Al-xCu alloys was accepted as 45 min. In this way, it is foreseen to examine the characteristic changes of the alloys by reducing the number of experimental variables.

2.2 Cold Compression and Sintering Process

Commercially available Al and Cu powders with 44 μm dimensions and 99% purity were prepared according to the mixing ratios given in Table 1. To ensure the homogeneous distribution of Al and Cu powders in each determined mixture and to prevent aggregation among themselves, the mixing powders were placed in a specially designed ball mixer and mixed mechanically at 270 rpm for approximately 20 min. The mixture powders dispersed homogeneously in each other were preheated at 300 °C in an argon gas atmosphere. With this process, it is planned to partially break the oxide layer on the particles with the effect of temperature and remove the moisture content of the mixture powders.

Immediately after the preheating process was completed, the mixture powders were systematically stacked in a specially

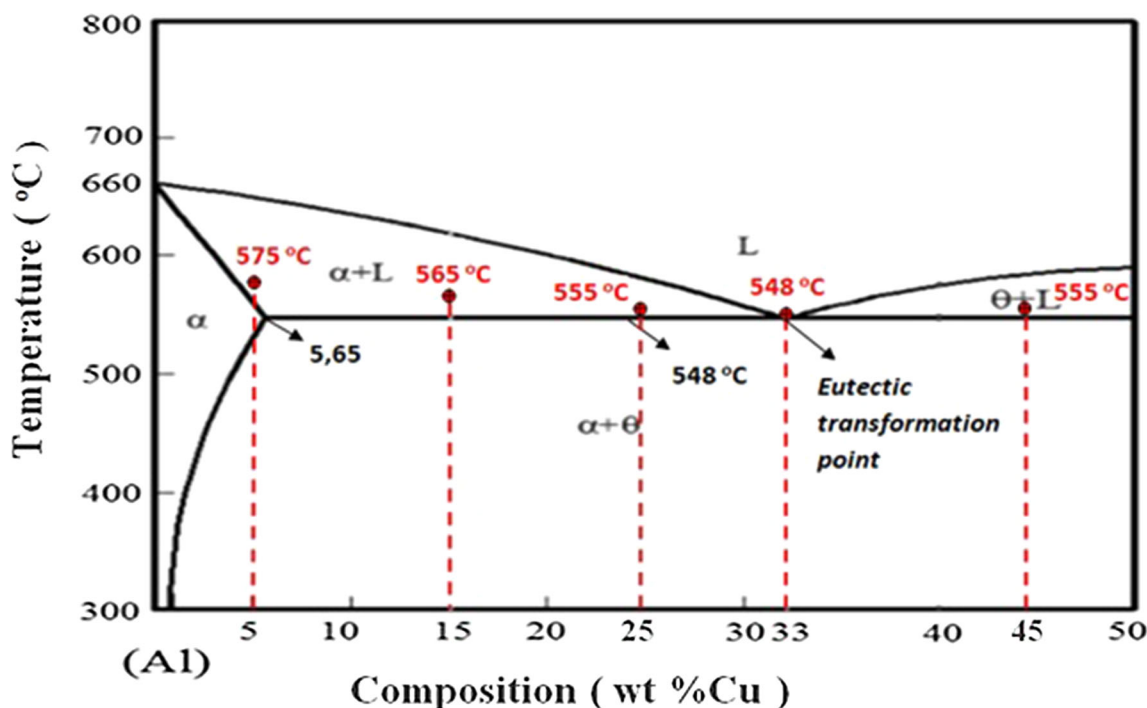


Fig. 1 Positions of Al-xCu alloy ratios and sintering temperatures on the binary equilibrium diagram.

designed die with a diameter of 20 mm and a height of 180 mm, the inner surfaces of which were lubricated with zinc stearate. After the stacking process, the one moving upper punch was placed in the die and the compression process was carried out at room temperature using a uniaxial compression device. In the preliminary study to examine the effects of different pressure ratios on green compact, it was observed that a 600 MPa pressure ratio would be appropriate regarding microstructure and mechanical properties in the compression of Al-Cu mixture powders (Ref 21). The height of the green samples, obtained by compression at a 600 MPa pressure ratio, reached the range of 80-85 mm. After the cold compression application, five different green compact samples were obtained, five from each alloy ratio. In addition, pure Al samples were produced to clearly examine the structural changes of the alloys and compare them with each other.

To prevent the deformation occurring in the samples as a result of partial liquefaction during sintering in the three zones determined on the binary Al-Cu phase diagram, the green samples were taken into a specially prepared die and sintered in a furnace with a sensitivity of ± 2 °C at the previously determined temperatures, as shown in Fig. 2(a). Immediately after the sintering process, the die was removed from the furnace, and the samples were compressed under 5 MPa pressure and cooled in air, as shown in Fig. 2(b). Thus, the possible swelling effect on the samples after sintering and the resulting increase in the porosity ratio are prevented and the research is more reliable (Ref 22, 23).

2.3 Experimental Processes of Al-xCu Alloys

The samples obtained were sanded and polished and later etched in Keller chemical (1 ml HF, 1.5 ml HCl, 2.5 ml HNO₃,

Table 1 Mixing ratios of Al and Cu powders

Powder	Al-5Cu	Al-15Cu	Al-25Cu	Al-33Cu	Al-45Cu
Al wt.%	95	85	75	67	55
Cu wt.%	5	15	25	33	45

and 95 ml H₂O). Following this process, microstructure images of the samples were taken on a Nikon optical microscope and FEI scanning electron microscope (SEM). In addition, x-ray diffraction (XRD) and element energy-dispersive spectroscopy (point and mapping EDS) was used for the microstructure analysis of the produced samples. In the examination of microhardness and density values, the upper, lower and middle parts of the produced samples were used and their average values were taken. Microhardness values were calculated based on average values obtained from 20 iterative measurements under a load of 100gf with the Wellmess WM-MCV-1A device. The Archimedes method with six different samples was used to calculate the experimental density of the green and sintered samples, while Eq 2 was used to calculate the theoretical density (ρ_t) of the samples. w_c is the weight of the component element and ρ_c is the density of the component element. Thus, the theoretical density of the alloys was calculated using the mixing rule, which considers closed porosity. The density of the compounds formed after sintering was neglected in the calculation.

$$\rho_t = \frac{100}{\sum \frac{100 \cdot w_c}{\rho_c}} \quad (\text{Eq 2})$$

ZwickZ100 compression device was used to apply compression test to the prepared samples in accordance with ASTM E9 standards. For the wear test, samples with a diameter of 20 mm and a thickness of 10 mm were subjected to the wear test with three repetitions at 200 rpm rotation speed using 6 mm diameter abrasive balls at 200, 400 and 600 m distance under 10 N load, in accordance with ASTM standards. At each period of the wear test, the system was stopped, the sample and counterface disk removed, cleaned with organic solvents to remove traces of residue and surface contaminants, dried, and then weighed on a precision balance to determine weight losses. Finally, the electrical conductivity of the alloy samples was evaluated by measuring with the IACS (International Annealed Copper Standard) unit used for metals and alloys.



Fig. 2 (a) Sintering of Al-xCu alloys in the die and (b) pressure application after sintering.

3. Results and Discussion

3.1 Microstructural Properties of Al-xCu Alloys

In Fig. 3(a)-(f), microstructure images of Al, Al-5Cu, Al-15Cu, Al-25Cu, Al-33Cu, Al-45Cu green compact samples are displayed. As shown in Fig. 3(a), the green Al sample was regularly stacked with the effect of the compression pressure, but pores of approximately 20-45 μm in size were formed. In the microstructure image of the Al-5Cu alloy displayed in Fig. 3(b), it was observed that the Cu powders were dispersed in the structure, and the pore sizes became widespread by decreasing compared to the pure Al structure. In Fig. 3(c), it was observed that with the increase in the Cu content in Al, the pores formed around the Cu powders, and in Fig. 3(d), with the increasing alloy ratio, the Cu powders were positioned close to each other, causing pores around them. As shown in Fig. 3(e), (f), with the increasing alloy content, the Cu powders were deformed and came into contact with each other, and the pores were concentrated at these junction points.

SEM images and regional EDS analysis results of Al-xCu alloy samples to observe the phases (α and θ) formed in the microstructure after sintering are shown in Fig. 4(a)-(e). In the microstructure images of the alloys, different theta phase formation patterns are observed with the effects of Cu content and sintering temperatures. In the SEM image of the Al-5Cu alloy, the structure with dispersed Cu particles homogeneously distributed in the volume of the alloy was observed. This structure, called the precipitate distribution, is predicted to increase the strength of the alloy produced at a high rate.

Dendritic structure formations were observed in Al-15Cu and Al-33Cu alloy ratios, and it was seen that the dendritic structures formed in these two alloy ratios were very similar to each other except for the amount of thickness. While the dendritic center thickness of the Al-15Cu alloy in the hypo-eutectic region is approximately 2-10 μm , it is about 5-40 μm in the Al-33Cu alloy located in the eutectic point. The reason for this formation is the difference in sintering temperature and alloy ratios, and regular dendritic distributions will create superiority in material strength (Ref 24-26). The SEM image of the Al-25Cu alloy shows the presence of partially liquefied Cu particles and irregularly dispersed precipitates. In the Al-45Cu alloy, on the other hand, partial liquefaction and the formation of coarse dendritic structures were prominently displayed due to the increased Cu element in the alloy. In addition, regional EDS analysis results indicate that Al-xCu alloys have the desired mixing ratios.

In the light of the microstructure investigations on the different Al-Cu alloys produced, the Al-5Cu alloy had regular microstructural features, while the irregular structural features were formed in the Al-25Cu and Al-45Cu alloys. Similar results were obtained in the study conducted with the selective laser melting method (Ref 27).

To examine the obtained structures in more detail, the samples in hypo-eutectic, eutectic and hyper-eutectic regions were compared within themselves. In this context, point EDS analyses and mapping images of the Al-15Cu alloy in the hypo-eutectic region were performed and shown in Fig. 5. As a result of the point EDS analysis taken over the dendritic structure, the

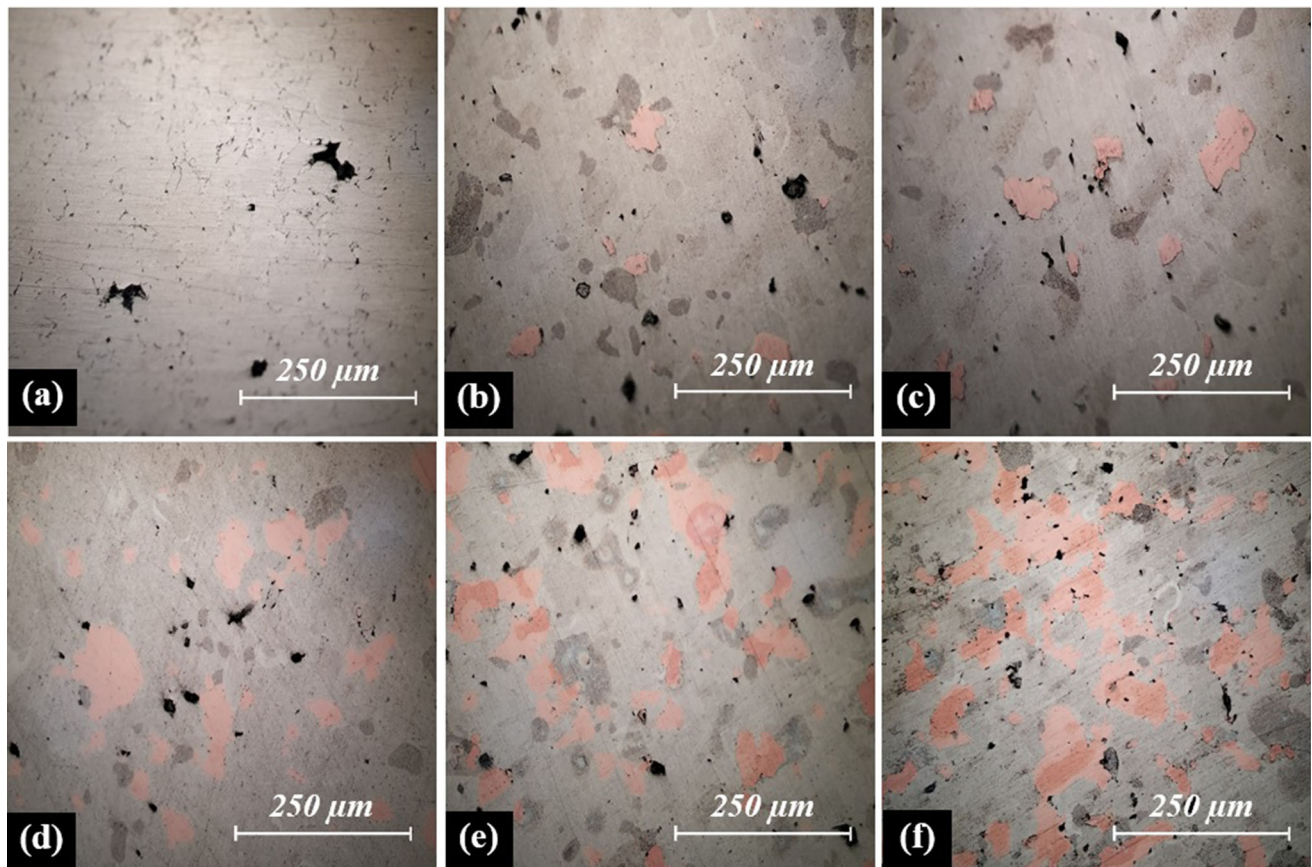


Fig. 3 Optical microscope images of green compacts (a) Al, (b) Al-5Cu, (c) Al-15Cu (d) Al-25Cu, (e) Al-33Cu, and (f) Al-45Cu.

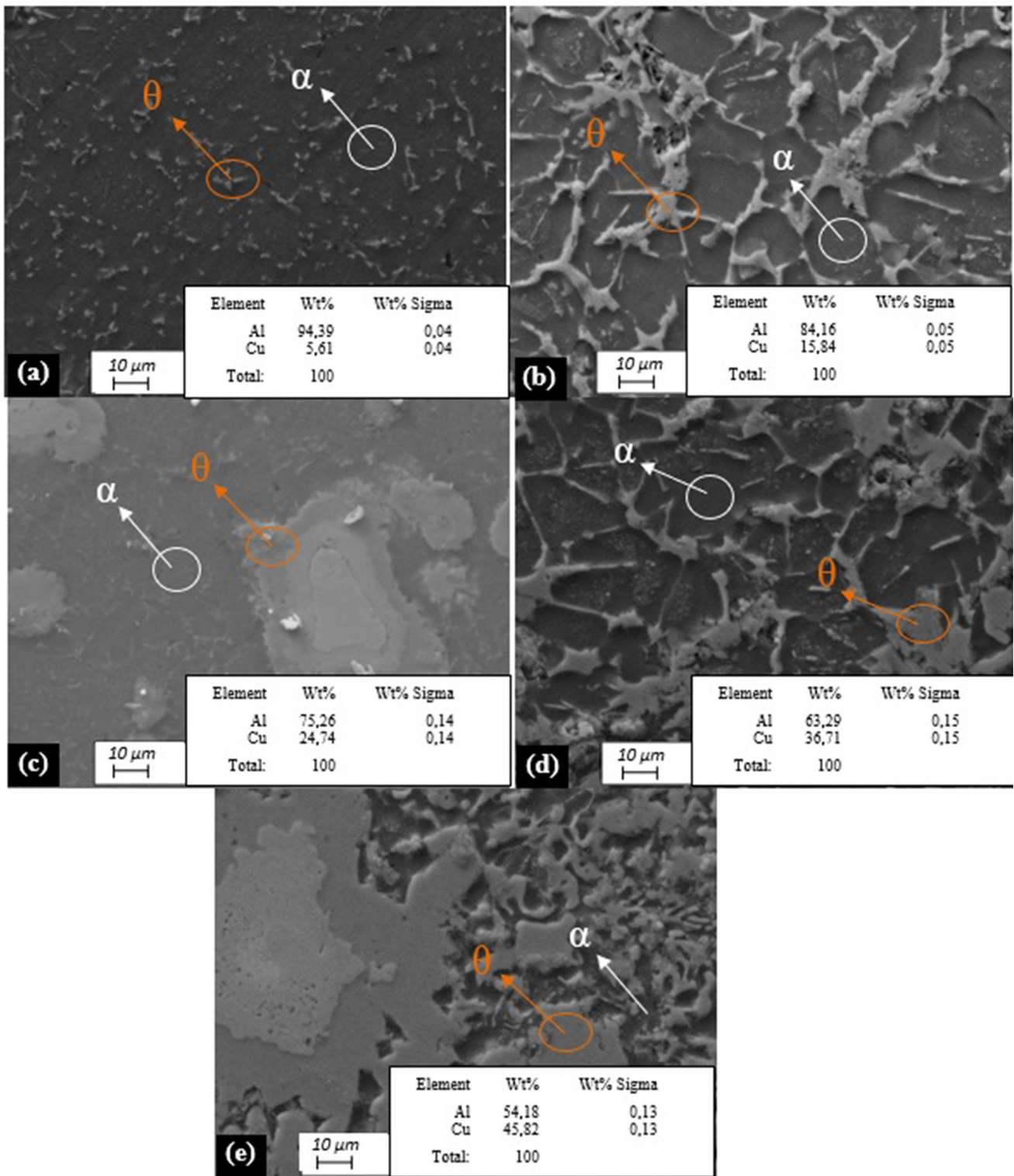


Fig. 4 SEM images and regional EDS analyzes of Al-xCu alloys after sintering, (a) Al-5Cu, (b) Al-15Cu, (c) Al-25Cu, (d) Al-33Cu, and (e) Al-45Cu.

intermetallic compound consisted of 54.18 wt.% Al and 45.82 wt.% Cu element. As a result of the point EDS analysis taken over the dendritic structure formed in the eutectic Al-33Cu alloy in Fig. 6, it was determined that the value of the element Cu increased by 13% compared to the Al-15 Cu alloy. Finally, the structure formed in the Al-45Cu alloy produced in

the hyper-eutectic region is examined in Fig. 7, and the values of the diffusional regions realized with partial melting were determined by EDS analyses taken from three different points. While there was approximately 73 wt.% Cu content in the central region of the gradient structure (spectrum 1), the values obtained from the center to the outer part (spectrum 2 and 3)

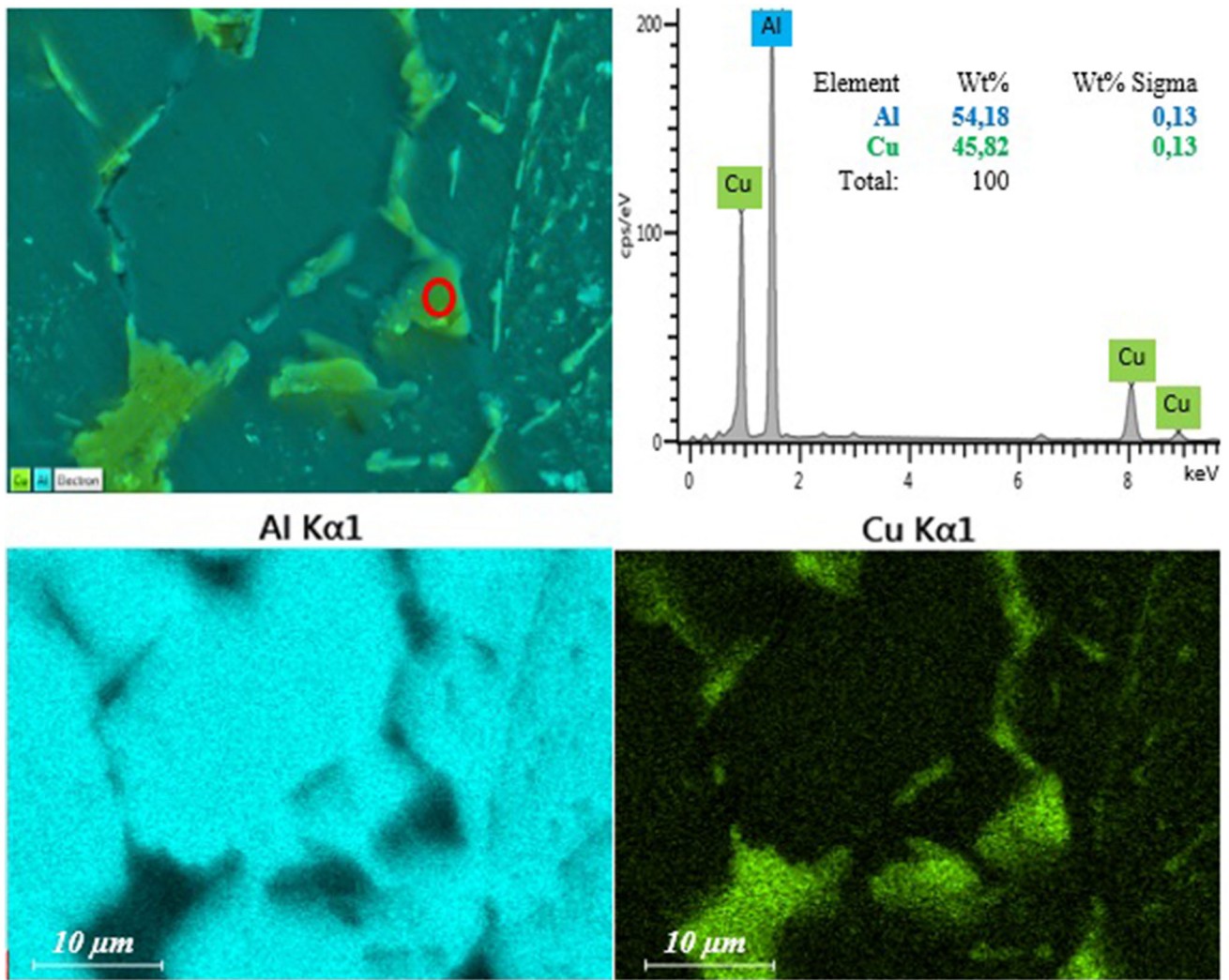


Fig. 5 EDS analysis (point and mapping) of the compounds formed in Al-15Cu alloy in the hypo-eutectic.

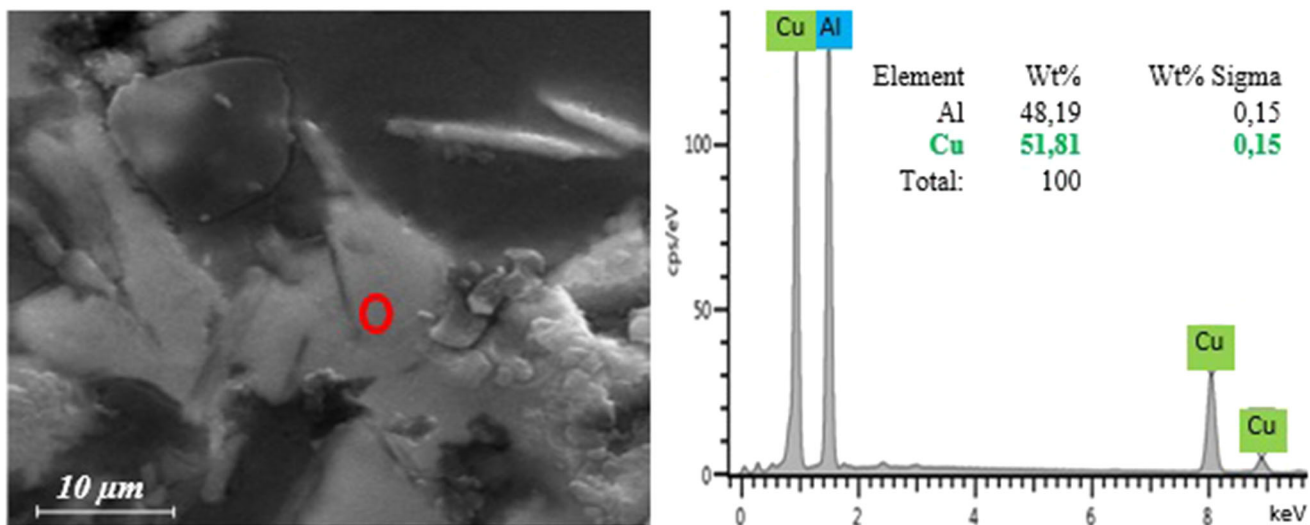


Fig. 6 EDS analysis of compounds formed in Al-33Cu alloy in the eutectic region.

were approximately the same as the values obtained in Al-33Cu compounds. The elemental values obtained show that the increase in Cu content causes a change in the rate of formation

of intermetallic compounds when passing from the hypo-eutectic region to the eutectic point. It was observed that the increase in Cu content did not change the elemental content

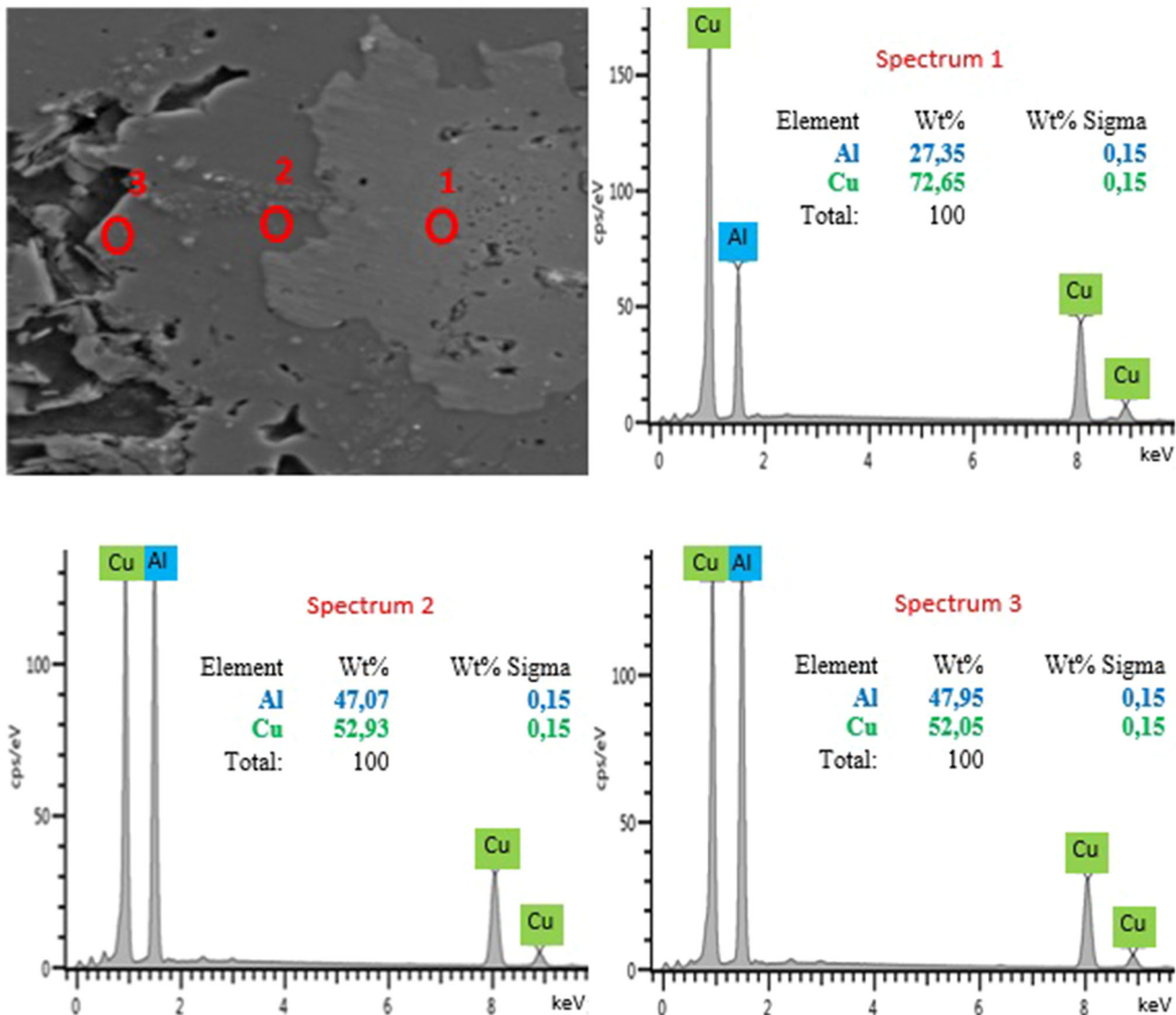


Fig. 7 EDS analysis of the structure formed in Al-45Cu alloy in the hyper-eutectic region.

value while passing from the eutectic point to the hyper-eutectic region, and it is thought that the reason for this is inactive copper particles.

To examine the phase properties of the precipitate distributions formed in the microstructure, XRD analysis was performed on the samples. The patterns obtained from this analysis are presented graphically in Fig. 8. As a result of the analysis, it was determined that the Al-Cu alloys produced phase formations rich in Al content and typically CuAl_2 phase. At the same time, the CuAl_2 phase distribution increased with increasing Cu content from Al-5Cu alloy to Al-33Cu alloy. In Al-45Cu alloy, on the other hand, it was observed that the peaks formed after XRD analysis became stable. The Cu phase is only prominently seen in Al-25Cu and Al-33Cu alloys. Thus, the dendritic structure obtained in the alloys included the CuAl_2 structure.

3.2 Densities of Al-xCu Alloys

Theoretical (ρ_t), green (ρ_g) and sintering (ρ_s) densities of Al-xCu alloys are shown in the graph in Fig. 9. In the graph obtained, the relative ratio between the ρ_g and ρ_t values of the

Al-5Cu alloy was 98%, while this ratio was determined as 95.5% for the Al-45Cu alloy. This variation between the ρ_g values of the alloy samples, which were made green compact by compression at the same pressure ratios, indicates that the increased Cu content causes porosity in the compression process. In the microstructure examinations of the green samples, it was observed that the increase in Cu content caused porosity in the microstructure. This observation coincided with the results obtained in the density measurements. In addition, it was determined that the ρ_s values of pure Al and Al-5Cu samples produced after sintering were close to the ρ_t values, while the difference between these values increased with the increase in Cu content in other alloys. However, ρ_s values are in the range of ρ_t to ρ_g values in all Al-xCu alloys. This evaluation process shows that the correct sintering parameters have been applied.

The graph obtained as a result of the calculation of the porosity ratios (P_p) of Al-xCu alloys after sintering is shown in Fig. 10(a). In the values calculated using Eq 3, it was observed that the porosity ratio P_p value increased with the increase in Cu content, and the highest P_p value among the alloys was

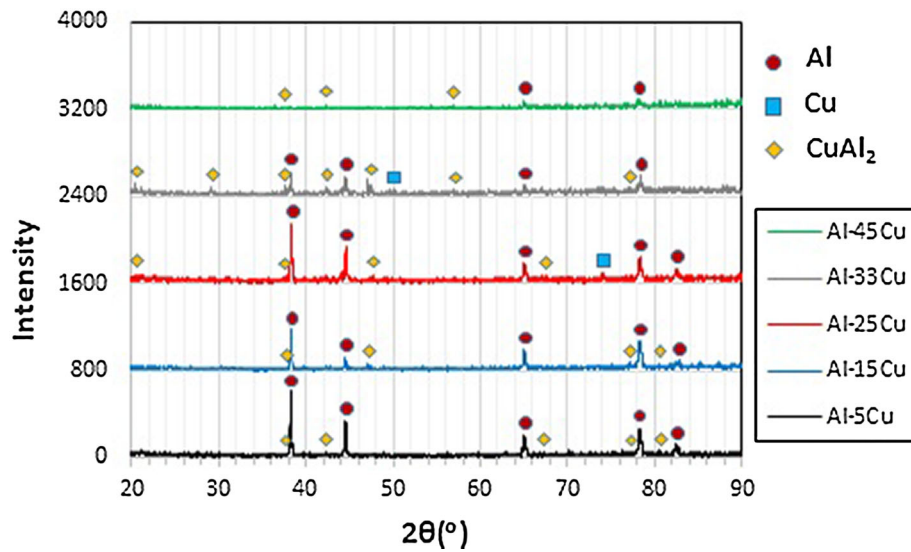


Fig. 8 XRD analysis patterns of Al-xCu alloys.

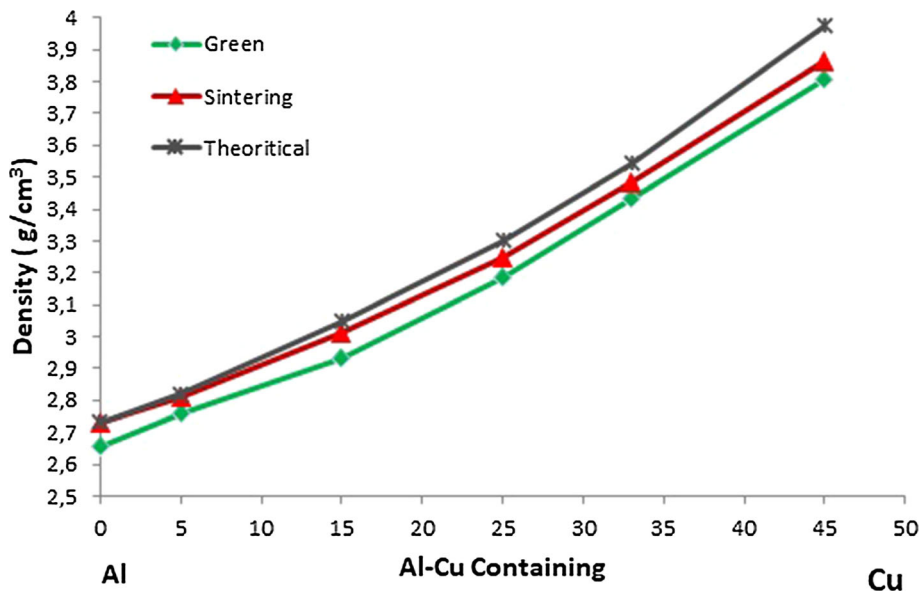


Fig. 9 Theoretical, sintering and green density values of Al-xCu alloys.

reached at 2.71% in the Al-45Cu alloy. This situation reveals that as the Cu content increases, the sintering temperatures should also increase. In addition, it can be stated that increasing copper content in Al-Cu alloys increases the area ratio of copper-rich compounds (CuAl_2). Thus, increased copper content may cause higher porosity (Ref 28). In Table 2, the density, porosity and densification values of Al-xCu alloys are presented.

$$P_p = 1 - \frac{\rho_s}{\rho_t} \quad (\text{Eq 3})$$

$$\Psi = 100 \cdot \frac{\rho_s - \rho_g}{\rho_t - \rho_g} \quad (\text{Eq 4})$$

In the graph shown in Fig. 10(b), the densification ratio (Ψ) values of Al-xCu alloys calculated using Eq 4 are displayed. As a result of the calculations, it has been seen that the best Ψ

value among Al-xCu alloys belongs to Al-5Cu alloy with 83.33%, but this value decreases with the increase in Cu content. The Ψ value of alloys other than Al-5Cu was approximately 50% on average.

3.3 Electrical Conductivity Properties

The electrical conductivity values of Al-xCu alloys are given in Table 3. It has been observed that the electrical conductivity values of Al-xCu alloys decrease as the ratio of Cu element added to the pure Al element increases. It can be argued that the reason for this is that the CuAl_2 phase increases in direct proportion to the increase in Cu addition and the electrical conductivity value of this phase are lower than the electrical conductivity value of Al and Cu elements. In addition, the content of Cu elements, which could not be converted into a liquid phase sufficiently in the Al-25Cu alloy due to the low sintering temperature, increased the electrical

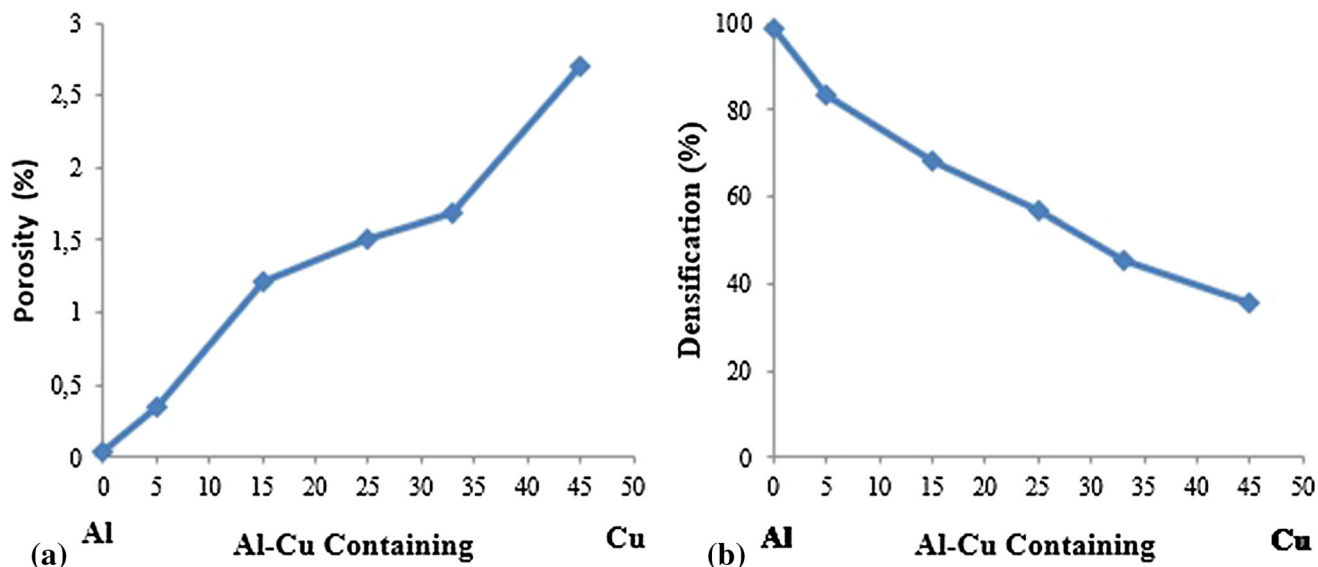


Fig. 10 After sintering of Al-xCu alloys, (a) porosity ratio and (b) densification ratio values.

Table 2 Density, porosity and densification values of Al-xCu alloys after sintering process

Al-xCu Alloys	Sintering temperature, °C	Green density, g/cm ³	Sintering density, g/cm ³	Theoretical density, g/cm ³	Porosity ratio, %	Densification ratio, %
Al	600	2.652	2.729	2.73	0.03	98.71
Al-5Cu	575	2.76	2.81	2.82	0.35	83.33
Al-15Cu	565	2.93	3.01	3.047	1.21	68.37
Al-25Cu	555	3.185	3.250	3.3	1.51	56.52
Al-33Cu	548	3.432	3.482	3.542	1.69	45.45
Al-45Cu	555	3.805	3.865	3.973	2.71	35.71

Table 3 Electrical conductivity of Al-xCu alloys

	Al	Al-5Cu	Al-15Cu	Al-25Cu	Al-33Cu	Al-45Cu
Electrical conductivity (%IACS)	38.9	37	25.2	28	22	19.5

conductivity value, which decreased gradually. However, this does not change the negative effects of Cu content on the electrical conductivity of the Al-xCu alloy (Ref 29).

3.4 Mechanical Properties

3.4.1 Microhardness. After the sintering process, the microhardness graph created by taking the average of the measurement values made at least six times from each of four different locations (Al, Cu, CuAl₂ and pores) formed in Al-xCu alloys is shown in Fig. 11. The hardness values of the alloys of Al-5Cu, Al-15Cu, Al-25Cu, which are located in the hypoeutectic region, were 81, 116 and 128 HV, respectively. In the literature review, it was determined that the hardness value of the Al-4.5Cu compact produced by the spark plasma sintering method was close to the hardness value of the Al-5Cu alloy produced in this study (Ref 30). In addition, the hardness value of the Al-33Cu alloy in the eutectic point was measured as 190 HV, while the hardness value of the Al-45Cu alloy in the hyper-eutectic region was determined as 310 HV. When the micro-

hardness values are examined, it is seen that there is an increase in the hardness value with the increase in the Cu ratio in the alloy, which is supported by similar studies (Ref 17). However, when the pure Al sample with a hardness value of 55 HV is accepted as the reference material, the Al-45Cu alloy reaches approximately six times higher hardness values.

Since the hardness value of the Cu element is approximately 100 HV, an average hardness value above this value is obtained in all alloys except Al-5Cu alloy. In the light of the investigations, the Cu content and temperature changes in the alloys obtained from different regions on the binary Al-Cu phase diagram lead to changes in the Al and Cu interaction, resulting in the formation of CuAl₂ compounds. These formations caused a significant increase in the hardness of the produced samples.

3.4.2 Wear Behaviors. To fully support the results of the positive changes in the hardness properties of Al-xCu alloys produced by the PM method, the wear test was applied to the alloys. In Fig. 12, the weight losses obtained in the wear test applied at 200, 400 and 600 m distances of the alloys produced

are given in graphically. It is observed that the wear resistance increases with the increase in Cu content after 0-200 m of the wear process. When the pure Al sample is accepted as a reference at this distance, it has been determined that the weight loss of the Al-5Cu alloy with the lowest wear resistance among the alloys decreases approximately four times compared to the reference material, and the weight loss of the Al-45Cu alloy with the best wear resistance decreases approximately 19 times. In a similar study, it was stated that the Cu content of Al alloys decreased weight loss after wear (Ref 31).

Weight losses of the alloys at a wearing distance of 200-400 m were generally slightly reduced compared to a distance of 0-200 m. The same situation was observed at 400-600 m wear distance, and it was determined that the alloy samples generally lost 2 mg of weight, while the Al-45Cu alloy had the best wear resistance with a weight loss of 1 mg at this distance. In Table 4, the total weight losses as a result of the wear test of Al-Cu alloys are given graphically. As can be seen from the

graph, it has been determined that the wear resistance of the alloys increases with the increase in Cu content and the weight loss of the Al-45Cu alloy, which has the best wear resistance, at 0-600 m is approximately 11 times less than that of pure Al. As a result of the analysis of the obtained values, the wear behavior of Al-xCu alloys was supported by hardness measurements.

3.4.3 Compression Test. The values obtained as a result of the compression test are shown graphically in Fig. 13. The maximum compressive strength values (σ_{max}) of the samples (Al, Al-5Cu, Al-15Cu, Al-25Cu, Al-33Cu, Al-45Cu) after sintering were 224, 659, 612, 480, 512, 493 MPa, respectively. It was observed that the compressive strength increased with the addition of 5% Cu to the pure Al element, but this strength value was lower at 15% and above Cu addition rates. As a result of the investigations, the compressive strength value of the Al-5Cu alloy increased approximately three times compared to the pure Al alloy. It is thought that this situation arises as a

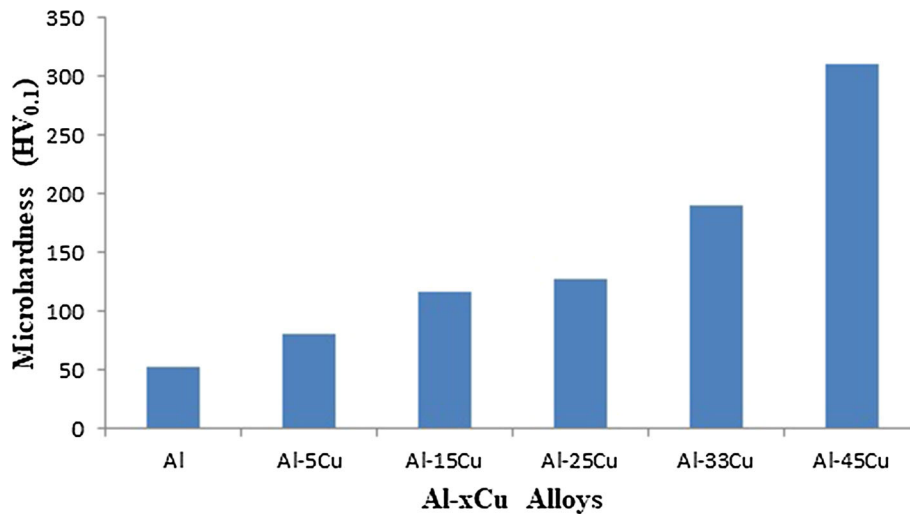


Fig. 11 Microhardness values of Al-xCu alloys after sintering.

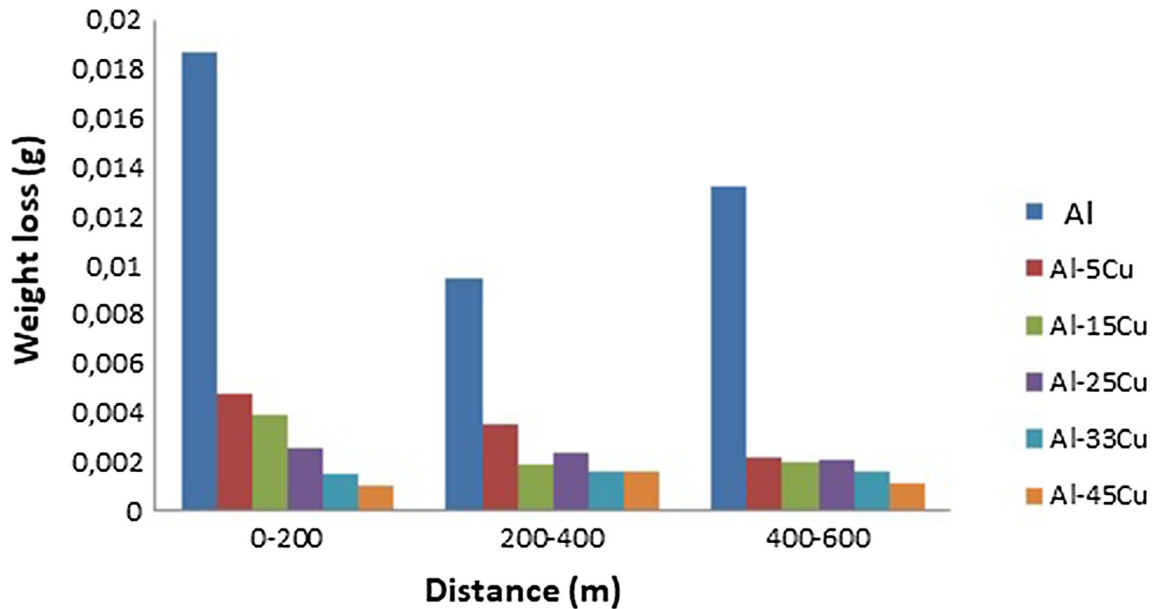
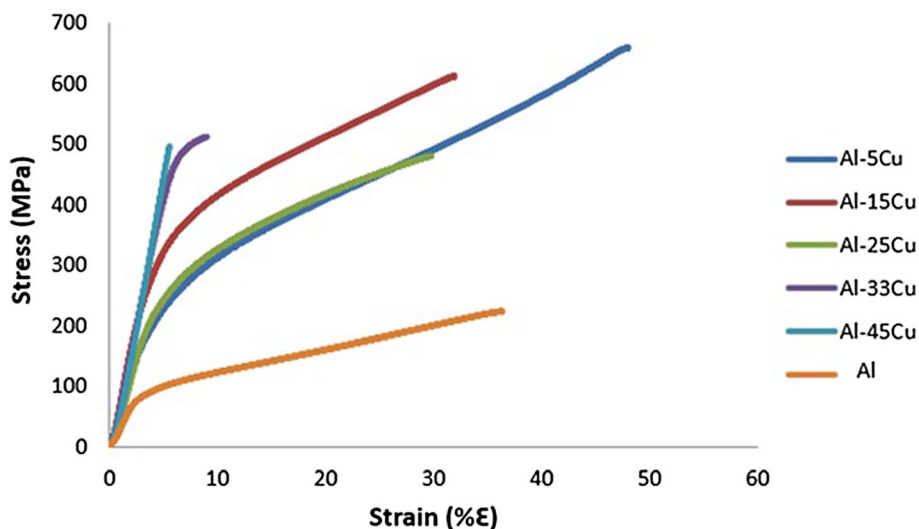


Fig. 12 Weight losses of Al-xCu alloys at different distances as a result of wear.

Table 4 Weight losses of Al-xCu alloys at different wear distances

Al-xCu Alloys	Weight loss 0-200 m, mg	Weight loss 200-400 m, mg	Weight loss 400-600 m, mg	Total weight Loss, mg
Al	18.7	9.5	13.2	41.4
Al-5Cu	4.8	3.5	2.2	10.5
Al-15Cu	3.9	1.9	2	7.8
Al-25Cu	2.6	2.4	2.1	7.1
Al-33Cu	1.5	1.6	1.6	4.7
Al-45Cu	1	1.6	1.1	3.7

**Fig. 13** Stress and strain curve of Al-xCu alloys after compression test.

result of the regular CuAl_2 distribution in the microstructure. Precipitation formations increase the strength of the material by preventing the movement of dislocations. The magnitude of this strengthening effect created by the precipitates on the material is naturally related to the microstructure properties of the precipitates (Ref 32).

Al-25Cu alloy, on the other hand, was determined as the alloy with the lowest compressive strength among the alloys whose production was completed. It is thought that the reason for this is the low sintering temperature and, as a result, insufficient liquefaction of the Cu element in the structure. In addition, the deformation before fracture ($\% \epsilon_{\text{max}}$) of Al-xCu alloys (Al, Al-5Cu, Al-15Cu, Al-25Cu, Al-33Cu, Al-45Cu) is 36, 48, 32, 29, 9, and 5.5%, respectively. Thus, it was revealed that there was a decrease in the amount of deformation with the increase in the Cu content among the alloys produced. This situation emerges as a normal occurrence in the light of the values obtained in hardness measurements. Al-45Cu alloy, which has the highest hardness value, is superior to other alloys regarding rigidity, and its ductility is at a minimum level.

Given the compression test properties, it was revealed that the best alloy sample was Al-5Cu. At the same time, it should not be ignored that the Al-5Cu alloy has superior properties regarding both strength and ductility when compared to the pure Al sample, which is accepted as a reference, and this is the most desirable property in material production.

4. Conclusion

In the present study, the changes in microstructure, and physical and mechanical properties of Al-xCu alloys produced by the PM method in the critical transformation regions of the binary Al-Cu phase diagram were investigated. The results obtained in this context are summarized as follows:

- In microstructural investigations of Al-xCu alloys produced at different alloy ratios and sintering temperatures, CuAl_2 precipitates in different formations were observed depending on the Cu content. In addition, the most regular precipitate formation among Al-xCu alloys occurred in Al-5Cu (575 °C) alloy, and partial liquefaction occurred in Cu particles in Al-25Cu (555 °C) and Al-45Cu (555 °C) alloys. In EDS analysis, it was determined that the amount of Cu element in the compound content formed in the hypo-eutectic region increased in the eutectic region, and the amount of Cu element in the compounds in the eutectic region and the hyper-eutectic region was almost at the same level. The findings suggest that this similarity is due to the inactive Cu particles formed because of insufficient sintering temperature or time.
- In the physical examinations made on Al-xCu alloys, the porosity ratio increased, and the densification ratio decreased with the increase in Cu content. The electrical conductivity values of the alloys decreased due to the increase in the ratio of CuAl_2 intermetallic compounds.

- With the increase in Cu content, the microhardness values of the alloys and their wear resistance increased. While the compressive strength and ductility values of Al-5Cu alloy had the best values among other alloys, the lowest ductility value was obtained in Al-45Cu alloy, and the lowest compressive strength value was obtained in Al-25Cu alloy.

Acknowledgments

This research was supported by Kahramanmaraş Sütçü İmam University Scientific Research Projects Coordination Unit with the project numbered 2021/1-16 YLS.

References

1. T. Qiu, M. Wu, Z. Du, G. Chen, L. Zhang, and X. Qu, Microstructure Evolution and Densification Behaviour of Powder Metallurgy Al-Cu-Mg-Si Alloy, *Powder Metall.*, 2020, **63**(1), p 54–63
2. K. Rajasekhar, V. Suresh Babu, and M.J. Davidson, Microstructural and Mechanical Properties of Al-Cu Functionally Graded Materials Fabricated by Powder Metallurgy Method, *Mater. Today Proc.*, 2019, **41**, p 1156–1159. <https://doi.org/10.1016/j.matpr.2020.09.157>
3. A.M. Sadoun, I.M.R. Najjar, M.S. Abd-Elwahed, and A. Meselhy, Experimental Study on Properties of Al-Al₂O₃ Nanocomposite Hybridized by Graphene Nanosheets, *J. Mater. Res. Technol.*, 2020, **9**(6), p 14708–14717
4. U. Avcı and Y.E. Erdoğan, Microstructure and Mechanical Properties of a Semi-Centrifugal Compression Processed Al6013 and Cu Bimetal, *Mater. Test.*, 2021, **63**(11), p 1058–1062
5. A.M. Sadoun, F.A. El-Wadoud, A. Fathy, A.M. Kabeel, and A.A. Megahed, Effect of through-the-Thickness Position of Aluminum Wire Mesh on the Mechanical Properties of GFRP/Al Hybrid Composites, *J. Mater. Res. Technol.*, 2021, **15**, p 500–510
6. A.F. Meselhy and M.M. Reda, Investigation of Mechanical Properties of Nanostructured Al-SiC Composite Manufactured by Accumulative Roll Bonding, *J. Compos. Mater.*, 2019, **53**(28–30), p 3951–3961
7. K. Rajasekhar, V. Suresh Babu, and M.J. Davidson, Interfacial Microstructure and Properties of Al-Cu Functionally Graded Materials Fabricated by Powder Metallurgy Method, *Mater. Today Proc.*, 2021, **46**, p 9212–9216
8. A. Mohamed, M.M. Mohammed, A.F. Ibrahim, and O.A. El-Kady, Effect of Nano Al₂O₃ Coated Ag Reinforced Cu Matrix Nanocomposites on Mechanical and Tribological Behavior Synthesis by P/M Technique, *J. Compos. Mater.*, 2020, **54**(30), p 4921–4928
9. K. Kim, A. Roy, M.P. Gururajan, C. Wolverton, and P.W. Voorhees, First-Principles/Phase-Field Modeling of Θ' Precipitation in Al-Cu Alloys, *Acta Mater.*, 2017, **140**, p 344–354
10. T. Balaram Reddy, P. Karthik, and M. Gopi Krishna, Mechanical Behavior of Al-Cu Binary Alloy System/ Cu Particulates Reinforced Metal–Metal Composites, *Results Eng.*, 2019, **4**, p 100046. <https://doi.org/10.1016/j.rineng.2019.100046>
11. A. Wąsik, B. Leszczyńska-Madej, M. Madej, and M. Goły, Effect of Heat Treatment on Microstructure of Al₄Cu-SiC Composites Consolidated by Powder Metallurgy Technique, *J. Mater. Eng. Perform.*, 2020, **29**(3), p 1841–1848
12. M. Aravind, P. Yu, M.Y. Yau, and D.H.L. Ng, Formation of Al₂Cu and AlCu Intermetallics in Al(Cu) Alloy Matrix Composites by Reaction Sintering, *Mater. Sci. Eng., A*, 2004, **380**(1), p 384–393
13. W.S. AbuShanab, E.B. Moustafa, E. Ghandourah, and M.A. Taha, Effect of Graphene Nanoparticles on the Physical and Mechanical Properties of the Al2024-Graphene Nanocomposites Fabricated by Powder Metallurgy, *Results Phys.*, 2020, **19**(June), p 1–12
14. D.W. Wolla, M.J. Davidson, and A.K. Khanra, Studies on the Formability of Powder Metallurgical Aluminum-Copper Composite, *Mater. Des.*, 2014, **59**, p 151–159
15. V. Selvakumar, S. Muruganandam, and N. Senthilkumar, Evaluation of Mechanical and Tribological Behavior of Al-4%Cu-x%SiC Composites Prepared through Powder Metallurgy Technique, *Trans. Indian Inst. Met.*, 2017, **70**(5), p 1305–1315
16. K. Bharath, A.K. Khanra, and M.J. Davidson, Structural Properties Evaluation of Semisolid Extruded Al-Cu-Mg Powder Metallurgy Alloys, *Trans. Indian Inst. Met.*, 2019, **72**(4), p 1063–1074. <https://doi.org/10.1007/s12666-019-01581-8>
17. X.R. Shi, Z.S. Yu, and K.G. Prashanth, Solidification of Al-XCu Alloy under High Pressures, *J. Market. Res.*, 2020, **9**(3), p 2983–2991
18. H.F. El-Labban and E.R.I. Mahmoud, Modification of Microstructures for Hypoeutectic, Eutectic and Hypereutectic Al-Cu Binary Alloys, *Int. J. Cast Met. Res.*, 2015, **28**(2), p 81–88
19. C.P.A. Upadhyaya, Sintering Behaviour and Mechanical Properties of Al-Cu-Mg-Si-Sn Aluminum Alloy, *Trans. Indian Inst. Met.*, 2011, **64**(October), p 345–357
20. U. Avcı and A. Güleç, Effect of Different Sintering Temperatures on Microstructure and Mechanical Properties for Pure Al Material Produced by Powder Metallurgy, *El-Cezeri J. Sci. Eng.*, 2021, **2021**(1), p 462–470
21. M. Doğan and U. Avcı, Farklı Basınç Oranlarında Ham Pelet Haline Dönüştürülen Al-15Cu Alaşımının Mikro Yapı ve Mekanik Özelliklerinin İncelenmesi, *Düzce Üniv. Bilim ve Teknol Derg.*, 2022, **10**, p 1423–1432. <https://doi.org/10.29130/dubited.985076>
22. U. Avcı, The Analysis of Microstructure and Mechanical Properties in B₄C Reinforced Al-Zn Alloy Matrix Composites Manufactured Using a New Sintering Approach, *Russ. J. Non-Ferrous Met.*, 2022, **63**(3), p 344–359. <https://doi.org/10.3103/S1067821222030129>
23. C.D. Boland, R.L. Hexemer, I.W. Donaldson, and D.P. Bishop, Industrial Processing of a Novel Al-Cu-Mg Powder Metallurgy Alloy, *Mater. Sci. Eng., A*, 2013, **559**, p 902–908
24. A. Gökçe, F. Findik, and A.O. Kurt, Effects of Mg Content on Aging Behavior of Al₄CuXMg PM Alloy, *Mater. Des.*, 2013, **46**, p 524–531
25. A. Gökçe, F. Findik, and A.O. Kurt, Microstructural Examination and Properties of Premixed Al-Cu-Mg Powder Metallurgy Alloy, *Mater. Charact.*, 2011, **62**(7), p 730–735
26. A. Gökçe, F. Findik, and A.O. Kurt, Sintering and Aging Behaviours of Al₄CuXMg PM Alloy, *Can. Metall. Q.*, 2016, **55**(4), p 391–401
27. P. Wang, L. Deng, K.G. Prashanth, S. Pauly, J. Eckert, and S. Scudino, Microstructure and Mechanical Properties of Al-Cu Alloys Fabricated by Selective Laser Melting of Powder Mixtures, *J. Alloys Compd.*, 2018, **735**, p 2263–2266
28. D.K. Das, R. Barua, and S. Datta, Influence of Copper Addition on Mechanical Properties and Microstructure of Eutectic Al-12Si-Xcu Alloy Produced through Powder Metallurgy Process, *J. Adv. Mater. Eng., MAT J.*, 2020, **05**(02), p 1–5
29. S. Aksöz, Y. Ocağ, N. Maras, E. Çadırlı, H. Kaya, and U. Büyük, Dependency of the Thermal and Electrical Conductivity on the Temperature and Composition of Cu in the Al Based Al-Cu Alloys, *Exp. Therm. Fluid. Sci.*, 2010, **34**, p 1507–1516
30. H.K. Chandra Mohan, S. Devaraj, and K.S. Narayana Swamy, Microstructural and Mechanical Characterization of Spark-Plasma-Sintered Compact of Al-4.5 Wt.% Cu Alloy Powder, *J. Mater. Eng. Perform.*, 2021, **30**(4), p 2433–2438
31. A.M. Hassan, A.T. Mayyas, A. Alrashdan, and M.T. Hayajneh, Wear Behavior of Al-Cu and Al-Cu/SiC Components Produced by Powder Metallurgy, *J. Mater. Sci.*, 2008, **43**(15), p 5368–5375
32. C. Wolverton, Crystal Structure and Stability of Complex Precipitate Phases in Al-Cu-Mg-(Si) and Al-Zn-Mg Alloys, *Acta Mater.*, 2001, **49**(16), p 3129–3142

Publisher's Note Springer Nature remains neutral with regard to jurisdictional claims in published maps and institutional affiliations.

Springer Nature or its licensor (e.g. a society or other partner) holds exclusive rights to this article under a publishing agreement with the author(s) or other rightsholder(s); author self-archiving of the accepted manuscript version of this article is solely governed by the terms of such publishing agreement and applicable law.